Isolated Pd atoms in a silver matrix: Spectroscopic and chemical properties

Caroline Hartwig, Kevin Schweinar, Travis E. Jones, Sebastian Beeg, Franz-Philipp Schmidt, Robert Schlögl, and Mark Greiner

COLLECTIONS

Paper published as part of the special topic on Heterogeneous Single-Atom Catalysis

ARTICLES YOU MAY BE INTERESTED IN

Isolated Pd atoms in a silver matrix: Spectroscopic and chemical properties

View Online   Export Citation   CrossMark

Caroline Hartwig,[1] (ID) Kevin Schweinar,[2] (ID) Travis E. Jones,[3] (ID) Sebastian Beeg,[1] Franz-Philipp Schmidt,[1,3] (ID) Robert Schlögl,[1,3] and Mark Greiner[1,a)] (ID)

AFFILIATIONS

[1] Max Planck Institute for Chemical Energy Conversion, Mülheim an der Ruhr, Germany
[2] Max-Planck-Institut für Eisenforschung GmbH, Düsseldorf, Germany
[3] Fritz Haber Institute of the Max Planck Society, Berlin, Germany

Note: This paper is part of the JCP Special Topic on Heterogeneous Single-Atom Catalysis.
[a)]Author to whom correspondence should be addressed: mark.greiner@cec.mpg.de

ABSTRACT

Over the past decade, single-atom alloys (SAAs) have been a lively topic of research due to their potential for achieving novel catalytic properties and circumventing some known limitations of heterogeneous catalysts, such as scaling relationships. In researching SAAs, it is important to recognize experimental evidence of peculiarities in their electronic structure. When an isolated atom is embedded in a matrix of foreign atoms, it exhibits spectroscopic signatures that reflect its surrounding chemical environment. In the present work, using photoemission spectroscopy and computational chemistry, we discuss the experimental evidence from $Ag_{0.98}Pd_{0.02}$ SAAs that show free-atom-like characteristics in their electronic structure. In particular, the broad Pd4d valence band states of the bulk Pd metal become a narrow band in the alloy. The measured photoemission spectra were compared with the calculated photoemission signal of a free Pd atom in the gas phase with very good agreement, suggesting that the Pd4d states in the alloy exhibit very weak hybridization with their surroundings and are therefore electronically isolated. Since AgPd alloys are known for their superior performance in the industrially relevant semi-hydrogenation of acetylene, we considered whether it is worthwhile to drive the dilution of Pd in the inert Ag host to the single-atom level. We conclude that although site-isolation provides beneficial electronic structure changes to the Pd centers due to the difficulty in activating H_2 on Ag, utilizing such SAAs in acetylene semi-hydrogenation would require either a higher Pd concentration to bring isolated sites sufficiently close together or an H_2-activating support.

I. INTRODUCTION

During the last decade, single-atom alloys (SAAs) have gained considerable attention in heterogeneous catalysis research,[1] especially in selective hydrogenation reactions.[2–9] Usually, in a SAA, a dilute active metal of group 10 (Ni, Pd, Pt) is substituted in a noble metal host of group 11 (Cu, Ag, Au).[1–11] By this approach, only small amounts of the expensive active metal are used.[10]

For selective hydrogenation reactions, the ability of SAAs to dissociate H_2[11–13] and the spillover of hydrides from the active single sites to host metal atoms[11,14,15] are often discussed, which both influence the catalytic selectivity compared to the bulk active metal.

One selective hydrogenation reaction of considerable interest is the semi-hydrogenation of acetylene toward ethylene. Ethylene, the monomer for the large-scale industrial product polyethylene, is mainly produced by thermal cracking of hydrocarbons such as naphtha. During this process, small amounts (0.5%–2%) of acetylene are produced. Acetylene has to be diminished to the ppm level since it poisons the catalyst in the ethylene polymerization reaction.[16] Bimetallic AgPd alloys are industrially applied in this reaction[17–19] since they show increased selectivity toward ethylene compared to monometallic Pd catalysts, which also form side products, such as fully hydrogenated ethane and polymers, known as green oil, which poison the catalyst.[20–22] The superior performance of AgPd alloys in

the semi-hydrogenation of acetylene can be referred to their electronic structure, and the question arises how the catalytic properties of AgPd change when the dilution is pushed to the Pd site-isolation limit in a SAA.

The changes to catalytic properties upon alloying are generally classified as ensemble or ligand effects. Ensemble effects refer to the change in the coordination environment that occurs upon alloying, while ligand effects refer to the change in the electronic structure of metals when they are alloyed together.[23] Since ligand effects alter a metal atom's electronic structure, they can, in principle, be observed using electronic-structure sensitive spectroscopies, such as photoemission spectroscopy. In many alloys, differences in electro-negativity between the constituent elements give rise to a partial charge transfer.[24,25] Charge transfer can, in some cases, be observed by shifts in core-level XPS peaks (as long as the shift is not counter-acted by some other process, such as final-state effects).[26,27] Additionally, the electronic structure of the surrounding matrix can alter the screening properties of the photoemission process, giving rise to additional binding energy shifts[28] and possible changes in peak line shape.[29] Changes to the electronic structure might also be observed in the valence band spectra, which, to a first approximation, represent the cross section weighted valence projected density of states (PDOS) of the alloy and have an impact on the line shape and the core level shifts (CLSs).[26]

In some SAAs, the solute exhibits a very weak interaction with the matrix element, resulting in an electronically isolated metal site, where the solute's valence states resemble a free-atom state. This behavior can be seen in the d-band of the solute. While most transition metals in their pure form have d-bands that are several eV in width, in certain alloys, the solute's d-bands become very narrow.[5] This phenomenon has been shown recently for $Ag_{0.995}Cu_{0.005}$[30] and can also be found in older literature about transition metals containing impurities of another transition metal.[31–33]

In the present work, we demonstrate the spectroscopic characteristics of an $Ag_{0.98}Pd_{0.02}$ SAA and discuss how they are a consequence of its electronic structure and coordination environment by comparing with the computed photoemission signal (PES) of a free Pd atom. We also discuss whether the geometric and electronic site-isolation of Pd in the $Ag_{0.98}Pd_{0.02}$ model catalyst can manifest themselves in the catalytic behavior in the semi-hydrogenation of acetylene. This discussion contributes to an improved understanding of the nature of active sites in SAAs and single-atom catalysts.

II. EXPERIMENTAL SECTION

A. Synthesis of the $Ag_{0.98}Pd_{0.02}$ alloy

Quantitative amounts of Ag (slugs 3×3 mm^2, 99.99%) and Pd (granules < 7 mm, 99.95%) purchased from EvoChem were melted in a light oven, with a four-time re-melting process for homogenization. Afterward, the alloy was cold-rolled to a 1.6 mm thick foil and then annealed for 6 h at 800 °C to promote grain growth. The foil was cut into smaller pieces and mechanically polished step by step until a roughness of 1 μm was archived by using a diamond suspension as an abrasive. Subsequent annealing in 0.5 mbar O$_2$ at 500 °C led to the surface segregation of impurities such as Cu, K, S, Si, and Cl, which could then be removed by Ar$^+$ sputtering. This procedure

was repeated several times to clean the sample surface. The last step was heating in UHV at 500 °C. Additionally, an $Ag_{0.95}Pd_{0.05}$ alloy was prepared using the same procedure.

B. Polycrystalline Pd and Ag foil

The 0.1 mm thick Pd foil was purchased from Alfa Aesar (99.9%), and the Ag foil from Sigma-Aldrich (99.99%) is 0.5 mm thick. Both samples were cleaned by several Ar$^+$ sputtering and annealing cycles (in O$_2$, H$_2$ and vacuum).

C. XPS experiments

For the x-ray photoemission spectroscopy (XPS) measurements, two different near ambient pressure (NAP) XPS setups were used: (i) a lab source (NAP) XPS using monochromatic Al Kα (1487 eV) radiation and a Phoibos NAP-150 hemispherical analyzer from SPECS GmbH, and (ii) the (NAP) XPS setup at the UE56-2_PGM1 beamline at Bessy II, which is also equipped with a hemispherical analyzer from SPECS GmbH. For the experiments performed in this work, they were both operated in ultrahigh vacuum.

Before performing XPS measurements, the samples were Ar$^+$ sputter cleaned for 15 min. All spectra of the $Ag_{0.98}Pd_{0.02}$ alloy [except those of Figs. 3(c) and 3(d)] were measured using synchrotron radiation; thereby, excitation energies of 520 eV for Ag3d, 485 eV for Pd3d, and 200 eV for the valence band spectra were used. Reference spectra of the polycrystalline Pd and Ag foil were collected using the laboratory XPS (with Al Kα excitation). All peaks were analyzed using the CasaXPS software and fitted using a U2 Tougaard background.

D. STEM–EDX measurements

Scanning transmission electron microscopy (STEM) in combination with energy-dispersive x-ray spectroscopy (EDX) was performed using a Thermo Fisher Talos F200X at 200 kV. The focused electron beam was raster scanned across the region of interest—222 × 620 nm^3 large—and EDX spectra were collected by a four-quadrant detector (Super-X detection system, Thermo Fisher) from each scanning point (696 × 1940 spectra).

The scanning step size was 320 pm, and the acquisition time was 10 μs per pixel. 70 frames were acquired, and the collected EDX spectra of each frame were summed up, resulting in an improved signal-to-noise ratio. A beam current of 3.2 nA was used to resolve the low Pd signal within the sample. For quantification, background subtracted Pd–K and Ag–K lines were considered (using an empirical power law fitting). The peak areas were weighted by Brown–Powell ionization cross sections, as given within the analysis software (Velox 2.13, Thermo Fisher Scientific).

E. Calculations

The 4d PES spectra of the free Pd atom were computed using Quanty using Slater integrals and the spin–orbit coupling parameter computed for the neutral free atom at the Hartree–Fock level and empirical spectral broadening.[34] Density functional theory (DFT) calculations of the solids were performed using the Quantum ESPRESSO package version 6.4.1[35] at the PBE level using pseudopotentials from the PSlibrary[36] with a kinetic energy (charge density) cutoff of 60 Ry (600 Ry) for scalar relativistic and fully relativistic

simulations. AgPd SAAs were computed by substituting a single Ag atom with a Pd atom in $(2 \times 2 \times 2)$ and $(3 \times 3 \times 3)$ crystallographic supercells of face-centered-cubic (fcc) Ag, and relaxing all atom positions and lattice vectors until forces dropped below 10^{-3} a.u., the cell-pressure dropped below 0.5 kbar, and the change in total energy was below 10^{-4} Ry at the scalar relativistic level. Fixed geometry calculations were performed including spin–orbit coupling for Pd. The PDOS was generated with a broadening of 0.17 eV. Core level shifts were computed using the ΔSCF method.

III. RESULTS AND DISCUSSION

A. Homogeneity and electronic structure of Ag0.98Pd0.02 SAA in comparison with its plain constituents

Before going into the details of the valence states of the $Ag_{0.98}Pd_{0.02}$ alloy, it is necessary to verify that the Pd atoms are indeed present as geometrically isolated single sites in the Ag host. This is a challenging but inevitable part of all SAA studies. For the case of AgPd alloys, it is especially difficult since the constituents are neighboring atoms in the Periodic Table, and therefore, it is not possible to distinguish them by their contrast using high-angle annular dark-field (HAADF)-STEM. However, it is reasonable to expect that in low concentrations, Pd is present statistically as isolated atoms, since the AgPd phase diagram shows them to be completely miscible,[37] and that the heat of formation is always negative, indicating an attraction between Ag and Pd.[38] Additionally, DFT calculations reveal a positive aggregation energy for the formation of Pd dimers and trimers in an Ag host. From these studies, it can be concluded that Pd atoms prefer to be isolated.[39–41]

Further evidence for the Pd atom isolation was found in studies on AgPd alloys using a variety of methods including STM,[42] CO adsorption,[3] and a simulation method based on machine learning.[43]

To confirm these previous findings, we have used EDX mapping in a TEM on a thin piece of the alloy. Figure 1(a) shows

a dark field (DF) image of the analyzed sample position. The simultaneously collected EDX signal results in Ag and Pd maps as given in Fig. 1(b). The uniform distribution of the Pd signal in the EDX map indicates that the Pd is homogeneously distributed. The low Pd signal, and therefore high signal-to-noise ratio, hinders a clear interpretation on the very local scale (for a more detailed discussion on the homogeneity of Pd, see Fig. S1 in the supplementary material). However, integrating the EDX signal over the whole region shown in panels (a) and (b) gives a clear Pd peak [yellow arrows in Fig. 1(c)], which is identified by 2 ± 0.5 at. % [see Sec. II (the Experimental section) for details on the quantification].

Stronger evidence of the isolated nature of the Pd atoms can be seen in the XPS core level and valence band spectra, as explained here, with a discussion of the differences in the electronic structure of the Pd3d core level and the valence band states of the $Ag_{0.98}Pd_{0.02}$ alloy and pure Pd. Figure 2(a) shows the Pd3d spectrum of bulk metallic Pd. The peaks are asymmetric (asymmetry factor at 10% peak height is 0.4), with a tail extending to the high binding energy side of the main peak. The asymmetry is a result of intrinsic energy losses caused by interactions of the core-level electrons with the valence band electrons.[29,44] The degree of asymmetry depends on the local DOS at the Fermi level.[45] The DOS at the Fermi edge for bulk Pd is very high [Fig. 2(b)] because the Pd4d states are not completely filled, having an electron configuration of $4d^{9.5} 5s^{0.5}$.[45,46]

In contrast, the Pd3d line shape in the $Ag_{0.98}Pd_{0.02}$ alloy is quite symmetric (asymmetry factor of 0.95). The reason for the more symmetric shape is the low DOS around the Fermi level in the alloy. In the alloy, the Pd4d band becomes filled so that the states around the Fermi level in AgPd are primarily Ag5s [Fig. 2(b)]. Thus, few valence excitations are available to cause the energy loss that gives rise to peak asymmetry.

Additionally, it can be seen in the valence band spectra that the Pd4d valence states are well separated from the Ag4d states [Fig. 2(b)], which can be explained by weak wave-function mixing of the metal 4d states, as was previously also shown for a $Ag_{0.995}Cu_{0.005}$
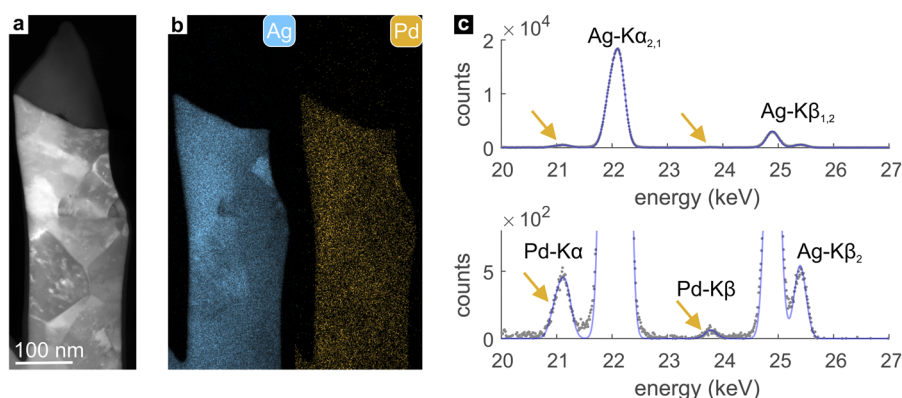

FIG. 1. STEM–EDX analysis: (a) dark field image of the Ag/Pd sample. (b) EDX maps showing the elemental distribution of Ag (left) and Pd (right) over the sample position as shown in (a). The color-coded signal corresponds to the net counts of the corresponding EDX signal (i.e., after background subtraction). (c) EDX spectrum extracted from the whole region shown in (a) and (b) (top). The Ag–K peaks are clearly resolved, while the Pd signal is hardly visible (yellow arrows) due to its low content of ~2 at. % relative to the Ag signal. Therefore, a magnified view of the same spectrum is shown in the lower panel, now clearly displaying the Pd-Kα but also Pd-Kβ peak. The blue lines are Gaussian fits to the experimental data (gray dots).
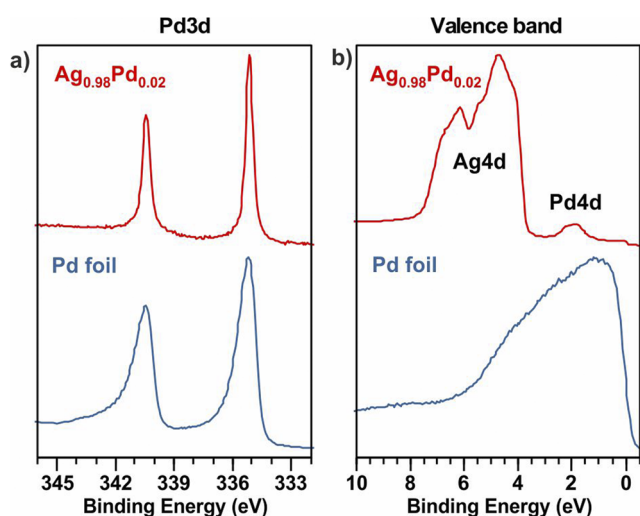
FIG. 2. Comparison of (a) the Pd3d and (b) the valence states of the $Ag_{0.98}Pd_{0.02}$ alloy with the polycrystalline Pd foil.

SAA,[30] and by DFT calculations of the DOS of multiple SAA combinations.[5] The weak wave-function mixing results from the fact that the filled Ag4d valence states are located below the Fermi level. For this reason, almost no hybridization of the Pd4d and Ag4d states is possible; hence, the Pd electrons are located at the Pd atom forming a narrow, electronically isolated virtual bound state.[26]

Spectroscopic evidence of the homogeneity of the AgPd SAA can be found in the XPS line shape of the $Ag3d_{5/2}$ and the $Pd3d_{5/2}$ signals. As mentioned above, the line shape depends on the DOS at the Fermi level. In a homogeneous alloy, the components share the same DOS; therefore, they are expected to have similar line shapes

(in the absence of satellites on the solute atom). Figures 3(a) and 3(b) show a comparison of the line shape of Pd3d in $Ag_{0.98}Pd_{0.02}$ with that of Ag3d. Here, we fit the $Ag3d_{5/2}$ signal using the generalized Voigt line shape (LF in CasaXPS 2.3.23) on a Tougaard background. The exact same line shape was then used to fit the $Pd3d_{5/2}$ signal. As one can see in Figs. 3(a) and 3(b), an identical line shape can be used to fit both signals reasonably well, suggesting that they share a similar electronic structure, both in terms of initial-state and final-state.

Further indication for successful alloying is the core level shift (CLS) of the $Ag3d_{5/2}$ peak from 368.20 eV for pure Ag to 368.18 eV for $Ag_{0.98}Pd_{0.02}$ and 368.10 eV in the case of an $Ag_{0.95}Pd_{0.05}$ alloy. The peak shift goes hand-in-hand with an increase in the FWHM of $Ag3d_{5/2}$ from 0.70 eV for the Ag reference sample to 0.78 eV for the $Ag_{0.95}Pd_{0.05}$ sample [Fig. 3(c)]. Calculations of the CLS of Ag, as a function of the Pd neighbors, revealed a linear correlation toward lower binding energies of Ag.[26,47] The CLS of Ag3d toward lower binding energies, as the concentration of Pd increases, can be explained by charge transfer of Ag5s states to Pd4d states, as it can also be observed for the metal-to-oxygen charge transfer in oxidized Ag.[48] This negative shift is attributed to final-state effects, where the screening charge has bonding 5s character.[48] The impact of charge transfer is very weak for the highly diluted $Ag_{0.98}Pd_{0.02}$ alloy, where the CLS accounts only to 0.02 eV. As the concentration of Pd in Ag increases, additional hybridization effects lead also to a more negative shift of the Ag3d states.[26] The broadening of the Ag core level signal suggests that there are distinct CLSs for Ag atoms adjacent to Pd atoms and Ag atoms not in the direct neighborhood of Pd atoms.[47]

Additionally, slight differences in the binding energy of the $Pd3d_{5/2}$ core level could be observed from 335.04 eV for the pure Pd metal, 335.12 eV for $Ag_{0.98}Pd_{0.02}$, to 335.06 eV for $Ag_{0.95}Pd_{0.05}$ [Fig. 3(d)]. It should be mentioned that the CLS does not show a linear trend in the case of Pd, and it is important to distinguish between initial- and final-state effects. Due to the higher density of states
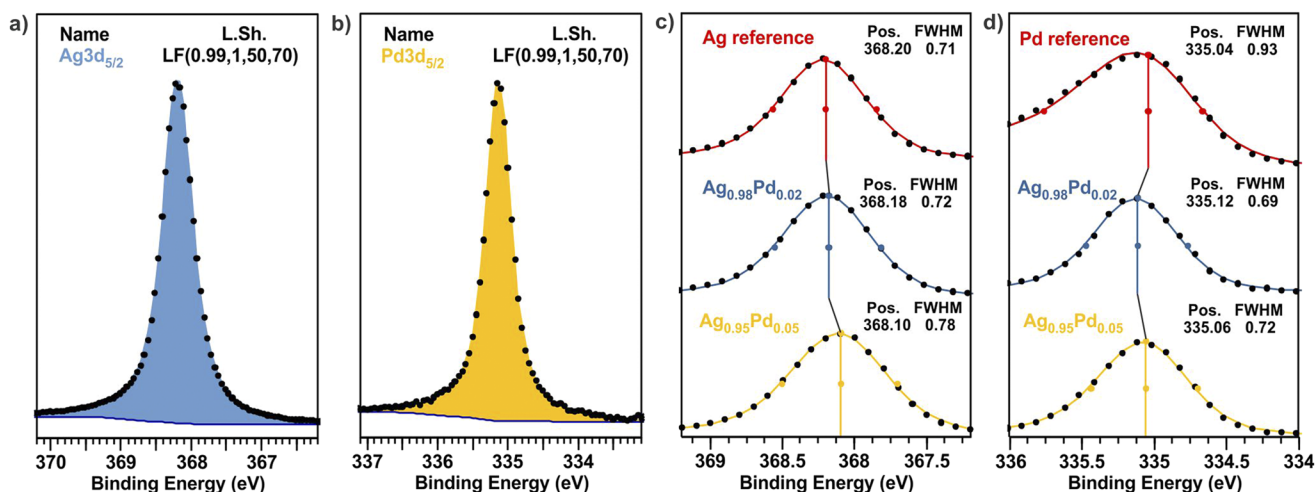
FIG 3. Fitting of the $Ag3d_{5/2}$ (a) and $Pd3d_{5/2}$ (b) signals of $Ag_{0.98}Pd_{0.02}$ using the same line shape. An identical line shape is a sign for a homogeneous alloy because it means that the constituents share the same DOS. CLS and peak broadening of $Ag3d_{5/2}$ (c) and $Pd3d_{5/2}$ (d) due to alloying in an $Ag_{0.98}Pd_{0.02}$ and $AgPd_{0.58}Pd_{0.05}$ alloy compared to pure Ag and Pd. The colored points represent the FWHM.

near the Fermi level in the bulk Pd metal, compared to $Ag_{0.98}Pd_{0.02}$, Doniach–Sunjic core-hole screening,[44] which leads to asymmetry, plays a more dominant role in the Pd metal than in $Ag_{0.98}Pd_{0.02}$, where there is almost no screening charge at the Fermi level. Since bulk Pd and Pd in the AgPd SAA have very different DOS, it is not straightforward to directly compare and discuss the Pd3d peak positions of the Pd metal and $Ag_{0.98}Pd_{0.02}$.

In contrast, $Ag_{0.98}Pd_{0.02}$ and $Ag_{0.95}Pd_{0.05}$ have very similar valence electronic structures, and the Pd3d peak positions can be more directly compared. In this case, we see that the peak position shifts slightly toward lower binding energy, as the Pd concentration increases.

As mentioned above, the Pd4d virtual bound state in AgPd SAA shifts below the Fermi level and becomes very narrow due to the localization of the Pd electrons around the atom because of the weak wave function mixing of the Ag4d and Pd4d states. One would expect that this effect would lead to a decrease in the binding energy for the Pd3d core levels in the initial state since the Pd4d band becomes more populated and more negatively charged due to the charge transfer of Ag5s states toward Pd4d states. However, in an AgPd SAA, the screening charge at the Fermi level changes its character from 4d orbitals with a high DOS in pure Pd to sp character from the neighboring Ag atoms with low DOS at the Fermi level. The low DOS at the Fermi edge leads to very little core-hole relaxation and hence to a pronounced final-state effect. As a consequence of the reduction in screening charge, the shift toward higher binding energies becomes more pronounced as the Pd concentration decreases toward infinite dilution.[26] Therefore, the positive shift is higher for $Ag_{0.98}Pd_{0.02}$ than for $Ag_{0.95}Pd_{0.05}$. In order to validate the measured CLS, the CLS of AgPd SAAs in comparison to Pd bulk was computed by substituting a single Ag atom with a Pd atom in $(2 \times 2 \times 2)$ and $(3 \times 3 \times 3)$ crystallographic super-cells of fcc Ag, revealing $Ag_{31}Pd_1$ $(Ag_{0.97}Pd_{0.03})$ and $Ag_{107}Pd_1$ $(Ag_{0.99}Pd_{0.01})$, respectively. For both supercells, the computed $Pd3d_{5/2}$ CLS is 0.08 eV, which is precisely the shift we measured for the $Ag_{0.98}Pd_{0.02}$ alloy [Fig. 3(d)]. This result demonstrates that no further CLS and electronic structure changes are expected when diluting Pd below 3 at. % in Ag.

It should be noted that the discussed CLSs for Ag- and $Pd3d_{5/2}$ states are very small, but previous researchers performed experimental and theoretical calculations of the CLS in Ag–Pd alloys over the whole concentration range.[26,49] Thereby, they found that the effect of inter-atomic d-electron charge transfer, which is often discussed as origin for CLSs, is negligible for Ag–Pd alloys.[26]

B. $Ag_{0.98}Pd_{0.02}$ valence band

In this section, we analyze in more detail the valence band of $Ag_{0.98}Pd_{0.02}$ measured with synchrotron radiation and discuss the findings by considering the literature from the 1960s to 1980s, where electronic structure changes induced by transition metal impurities in another transition metal were intensively studied.[31–33] The materials previously studied are, in principle, the same as the materials now referred to as SAAs. As shown in Fig. 2(b), the Pd4d states are well separated from the Ag4d states, but the FWHM of the Pd4d virtual bound states is 0.85 eV broader than it was for the $Ag_{0.995}Cu_{0.005}$ SAA (0.5 eV).[30] This observation opens the question: Which parameters have an impact on the width of the

valence states? Parameters giving rise to broadening are crystal field (d–d) coupling, s–d coupling, and spin–orbit coupling. In general, the d-band width increases along a row of the Periodic Table and reaches its maximum in group 5, and then it decreases again as the d-band becomes filled. Along the column from 3d to 5d elements, the d-band width increases due to more interacting electrons.[50] Consequently, the fact that Pd is a 4d and Cu is a 3d element and that Pd is in group 10, whereas Cu is in group 11 leads to broader Pd valence states.

Norris and Meyers claimed already in 1971 that even at infinite dilution, there is broadening of the Pd4d bound states due to the spin–orbit splitting and the s–d coupling. The d–d interactions (crystal field effects) can be neglected in the case of transition metal impurities in the host metal.[31] In 1985, van der Marel et al. investigated experimentally (UPS) and theoretically Pd and Pt induced changes in noble-metal density of states.[30] From the UPS results of a $Ag_{0.97}Pd_{0.03}$ alloy, it became clear that spin–orbit splitting plays a role for the broadening of the Pd4d valence states. Consequently, we fitted the Pd4d states of the $Ag_{98}Pd_{02}$ sample using two signals with the typical area ratio for 4d states of 2:3. In Fig. 4(a), it can be seen that this approach results in a good fit for the Pd4d signal shape. The $Pd4d_{5/2}$ and the $Pd4d_{3/2}$ peak in the fit are centered at a binding energy of between 1.8 and 2.2 eV. The positions are identical with the one observed in the literature for the $Ag_{0.97}Pd_{0.03}$ alloy.[30] In that publication, the authors found an identical FWHM of 0.8 ± 0.1 eV for the entire Pd4d signal. Furthermore, they theoretically calculated the valence band using a spin–orbit coupling and an s–d coupling parameter but no crystal field coupling parameter. This agrees with the predictions of Norris and Meyers that only spin–orbit coupling and s–d interactions have an influence on the broadening.[33]

To estimate, if the Pd atoms in the $Ag_{0.98}Pd_{0.02}$ alloy really behave like electronically isolated free-atoms sites, as it was predicted for the free-atom like $Ag_{0.995}Cu_{0.005}$ SAA,[30] one can compare the impurity valence d-states of the alloy with the calculated states of a single metal atom in the gas phase. The result of the calculations of the photoemission signal (PES) of such an isolated gas phase atom is shown in Fig. 4(b), which demonstrates that spin–orbit splitting plays a significant role in the valence states of a free Pd atom. The calculated splitting is 0.4 eV and is very close to the result obtained by fitting the Pd4d valence states in the XPS spectra [Fig. 4(a)]. Since spin–orbit splitting can account for the Pd4d band width, there might be very little hybridization between the Pd and Ag valence d-states, and therefore a free-atom like behavior of Pd.[51–53] To verify this proposition, the Pd4d PDOS of $Ag_{31}Pd_1$ was computed by fully relativistic DFT and a broadening of 0.17 eV [Fig. 4(d)]. It can be observed that there is also a weak Pd4d electron density between −6 and −3 eV, the range of the Ag4d states, and consequently, there is a small degree of hybridization between Ag and Pd. For comparison, the PDOS of bulk Pd is also plotted [Fig. 4(c)], which shows the width and the high DOS at the Fermi edge of Pd4d.

Our $Ag_{0.98}Pd_{0.02}$ SAA provides a reference for the often-discussed phenomenon of site-isolation, whereby in this case, geometric site-isolation is accompanied by electronic site-isolation. In Sec. III C, we will discuss the effect of the geometric and electronic site-isolation on the catalytic performance of AgPd SAAs in the selective hydrogenation of acetylene.
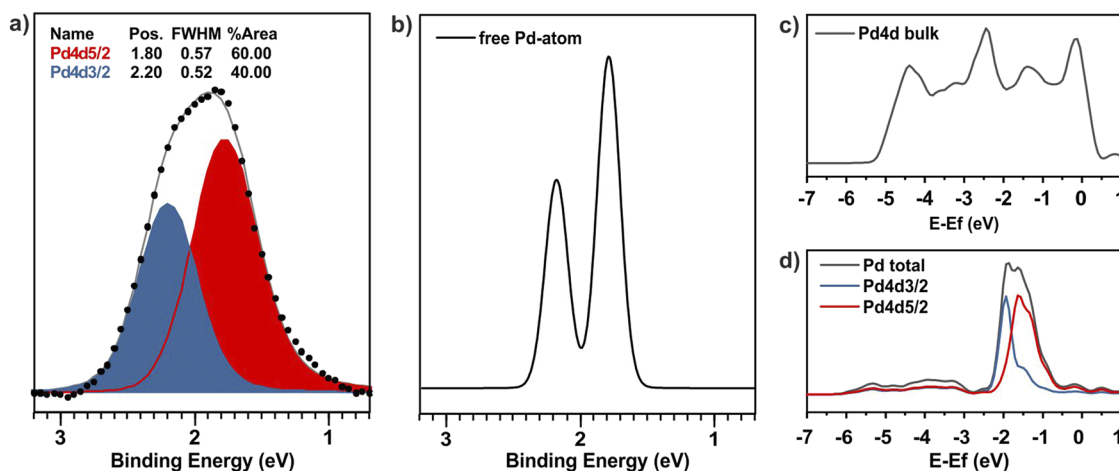
FIG. 4. (a) The Pd4d valence states are fitted using two peaks due to spin–orbit splitting, and thereby, the typical area ratio of 2:3 is used. (b) Calculated PES of a free Pd atom with spin–orbit splitting. The energy scale is adjusted to the XPS experiment. The calculated splitting is 0.4 eV, closely matching the splitting in the measured signal. (c) PDOS of bulk Pd. (d) Pd4d PDOS of $Ag_{31}Pd_1$ including the spin–orbit splitting of $Pd4d_{3/2}$ and $Pd4d_{5/2}$.

C. Discussion of the catalytic properties of AgPd SAA in selective acetylene hydrogenation

Previous work has shown that bimetallic AgPd alloys can exhibit increased selectivity toward ethylene, compared to monometallic Pd catalysts, which also form side products, due to its high activity.[20,21,54,55] Those side products are fully hydrogenated ethane and polymers, known as green oil, which poison the catalyst.[20–22] It is believed that alloying Pd with Ag increases ethylene selectivity for two reasons: (i) it hinders the formation of sub-surface hydrogen, which is responsible for the full hydrogenation pathway toward ethane,[21,55,56] and (ii) it weakens the binding strengths toward all surface intermediates, leading to increased desorption of the desired product, ethylene.[57–59] The latter effect is because the d-band of Pd becomes filled due to alloying,[26,60,61] which weakens the adsorption of π-electron donors such as acetylene and ethylene, since they can donate fewer electrons into the Pd d-band.[20] In the present work, the valence band spectra (Fig. 4) indicate a full d-band for Pd, strongly supporting this model. Due to the filled d-band, the ethylene desorption barrier becomes lower than the hydrogenation barrier,[57] and also C–C coupling, which leads to the formation of green oil, is unlikely to occur.[62]

On the other hand, one can say that Ag is inactive in acetylene hydrogenation since (defect free) Ag ensembles can neither adsorb acetylene[63,64] nor activate H_2.[65] Therefore, although the selectivity increases when Pd is alloyed with Ag, the overall activity of the selective hydrogenation reaction decreases with increasing Ag content. Consequently, the question arises: Which Ag:Pd ratio is ideal to catalyze the reaction. Khan and co-workers thoroughly summarized the requirements of an ideal AgPd catalyst:[21] *"the Pd–Ag system should have, on the one hand, the Pd-rich surface to dissociate hydrogen and catalyze reaction with acetylene and, on the other hand, an Ag-rich core to prevent hydrogen migration into the particle."* In their work, they showed that an AgPd model catalyst became inactive at very

high Ag surface coverages. In essence, if H_2 is activated at Pd sites and if acetylene adsorbs at Pd sites, then in the case of site-isolation, the adsorbates must be able to diffuse to each other for the reaction to occur.

Tierney and co-workers demonstrated theoretically[13] and by STM experiments[14] that H_2 dissociation can occur on isolated Pd sites of CuPd and AuPd SAAs; however, they found that only for CuPd SAAs, a subsequent spillover of hydrides to the host atoms (Cu) was possible.[11,14,15] Previous DFT calculations of the formation energy of adsorbed H atoms by Darby *et al.* revealed formation energies of 0.16 eV for a Ag(111) surface and −0.12 eV for a Pd-doped Ag(111) surface, whereas the energies for a Pd-doped Cu(111) and plain Cu(111) surface were between −0.27 and −0.26 eV, respectively.[66] These values verify why spillover of H atoms is likely to occur on CuPd SAAs but not on AgPd. Thus, we expect that without H spillover, isolated Pd sites in AgPd SAAs must be sufficiently close to one another for semi-hydrogenation to occur.

The work of Armbrüster and co-workers on Ga–Pd intermetallics demonstrated such an effect.[67–69] In that example, Pd and Ga are covalently bonded in a ordered crystal structure different from their constituents. Pd atoms are isolated in that no neighboring Pd atoms are present in the first coordination sphere.[68] The isolation of Pd sites hinders the formation of bulk hydrides and therefore avoids the formation of fully hydrogenated ethane,[69] while the close proximity of neighboring Pd atoms allows for adsorbates to encounter one another. The experiments show that $GaPd_2$ compared to GaPd has a 30-fold higher activity but the same selectivity (75%). The reason for the lower activity of GaPd is explained by the differences in the valence band structure. GaPd has a lower DOS at the Fermi edge (0.2 states eV^{-1} $atom^{-1}$), a lower lying d-band center (0.4 eV), and a narrower d-band width (0.9 eV) than $GaPd_2$,[67,68] and similar effects were observed for the Pd valence structure of AgPd in the present work. As mentioned above for the AgPd alloys, this electronic effect (i.e., filling of the d-states) enhances the

selectivity toward ethylene. In the case of AgPd, site-isolation could, in principle, still be obtained at Pd concentrations as high as 7 at. %—that is, one Pd atom for every 12 Ag atoms—such that in the fcc unit cell, the 12 atoms in the coordination sphere of a Pd atom are all Ag.

While close proximity of isolated sites can enable the semi-hydrogenation reaction to occur, the hydrogen uptake can also be increased by the support. In a previous study by Pei *et al.*, it was found that nanoparticle-sized, SiO$_2$ supported AgPd SAA catalysts were efficient and highly selective in the hydrogenation of acetylene in an excess of ethylene.[3] In their study, H$_2$ activation was likely enhanced by the presence of the support. Claus and co-workers' work on H–D exchange experiments on Ag/SiO$_2$, investigated by FTIR spectroscopy, revealed that even the bare SiO$_2$ support is able to activate H$_2$.[70,71] Other groups found that the H$_2$ dissociation on such non-reducible supports can be attributed to defect sites in the support.[72,73] It was experimentally shown that the H$_2$ activation increases for Ag nanoparticles on the SiO$_2$ support,[70,71] which could be explained by H–H exchange at the metal-support interface, where a H atom on the metal exchanges with a proton of the OH (silanol) group on the SiO$_2$ support.[73,74] Thereby, residual water molecules accelerate the H–H exchange.[73,75] Such metal–support interactions are possible for the supported AgPd/SiO$_2$ SAA catalysts, but not for the unsupported AgPd SAA foil examined in the present work. In addition, the AgPd nanoparticles in AgPd/SiO$_2$ might contain additional electron-deficient sites (defect sites and step and corner atoms), which lead to valence d-band vacancies and the facilitation of metal–H bond formation. Hence, Ag atoms in nanoparticles might be able activate H$_2$.[71,76]

In summary, a hydrogenation reaction requires two initial steps, the dissociation of hydrogen and the adsorption of the hydrocarbon (here acetylene). The alloying of Pd with another metal such as Ga or Ag hinders the formation of sub-surface hydrogen and also weakens the binding toward the desired product (ethylene) due to d-band filling, and both effects increase the selectivity.[51,52,69] The dissociation of hydrogen is possible at the single-atom Pd sites in SAAs, and for CuPd SAAs, a subsequent spillover of H atoms to the Cu host occurs, increasing the hydrogen uptake.[14,15] Additionally, the spillover enables the reaction of the hydrides with acetylene, which is adsorbed on the Pd sites. AuPd and AgPd SAAs are not expected to exhibit H$_2$ spillover to the host due to weak binding between H atoms and Ag or Au.[11,13,14,66] Hence, the H atoms cannot approach and react with acetylene when the isolated Pd sites are far away from each other. In intermetallics such as GaPd, the Pd sites are also geometrically isolated but close enough for the adsorbates (H and acetylene) to react with each other.[67,69] In supported SAA catalysts, such as AgPd/SiO$_2$, H$_2$ can be activated at the defect sites of the support, and also electron-deficient Ag sites might activate H$_2$.[71] Those two effects increase the H$_2$ uptake and enable the reaction of H$_2$ and acetylene.

and discuss the ways in which its unusual free-atom like electronic structure is manifested in the measured spectra.

In particular, a comparison of the core level Pd3d line shapes of Ag$_{0.98}$Pd$_{0.02}$ and bulk Pd revealed a symmetric line shape for Pd3d in AgPd. The change in the line shape can be referred to the change in the local density of states at the Fermi level. Bulk Pd has very high density of states due to unfilled Pd4d states, which lead to asymmetric core-level line shapes. In contrast, the Pd4d states in the AgPd single-atom alloy are very narrow and filled and are hence shifted below the Fermi level. Furthermore, it was found that the Ag3d and Pd3d core-level states can be fitted using exactly the same line shape, which indicates that both metals share the same density of states and that the Pd atoms are homogeneously distributed in the alloy. Additionally, the Pd4d valence states in Ag$_{0.98}$Pd$_{0.02}$ are well separated from the Ag4d valence states. A comparison of the Pd4d valence states in the single-atom alloy with a calculated photoemission signal of a free Pd atom in gas phase showed good agreement. Consequently, there is a weak wave-function mixing of the Pd4d states with their surroundings, which verifies the electronic site-isolation of the Pd atoms.

We also discussed the effect of the site-isolation on the catalytic activity in acetylene hydrogenation. From the discussion, we concluded that the geometric and electronic Pd site-isolation in the inert Ag host should reduce the catalytic performance of the Pd atoms, as adsorbates (H$_2$ and acetylene) on isolated Pd sites of the Ag$_{0.98}$Pd$_{0.02}$ alloy would be too far away from each other to react. This issue can be avoided when the host material participates in the reaction, e.g., in CuPd SAAs, H$_2$ will be dissociated by the Pd sites followed by spillover to the Cu host.[15] In addition, defect sites in the support are able to activate H$_2$ and hence increase the H$_2$ uptake and the catalytic performance.[3,71,73]

SUPPLEMENTARY MATERIAL

Analysis of the homogeneity of Pd in Ag by STEM–EDX, catalytic investigation of AgPd SAA and Pd in acetylene hydrogenation, and information of the Ag3d to Pd3d ratio by heating the AgPd SAA in vacuum and in H$_2$ can be found in the supplementary material.

IV. CONCLUSION

Here, we have investigated an unsupported AgPd single-atom alloy foil using electron spectroscopy and computational chemistry. This Ag$_{0.98}$Pd$_{0.02}$ alloy is one of the few documented cases of electronic site-isolation in heterogeneous catalysis, and we demonstrate

DATA AVAILABILITY

The XPS data that support the findings of this study are openly available in Zenodo at https://doi.org/10.5281/zenodo.4481984, https://doi.org/10.5281/zenodo.4482000, and https://doi.org/10.5281/zenodo.4482138.

REFERENCES

[1] R. T. Hannagan, G. Giannakakis, M. Flytzani-Stephanopoulos, and E. C. H. Sykes, Chem. Rev. **120**, 12044 (2020).

[2] M. B. Boucher, B. Zugic, G. Cladaras, J. Kammert, M. D. Marcinkowski, T. J. Lawton, E. C. H. Sykes, and M. Flytzani-Stephanopoulos, Phys. Chem. Chem. Phys. **15**, 12187 (2013).

[3] G. X. Pei, X. Y. Liu, A. Wang, A. F. Lee, M. A. Isaacs, L. Li, X. Pan, X. Yang, X. Wang, Z. Tai, K. Wilson, and T. Zhang, ACS Catal. **5**, 3717 (2015).

[4] F. R. Lucci, J. Liu, M. D. Marcinkowski, M. Yang, L. F. Allard, M. Flytzani-Stephanopoulos, and E. C. H. Sykes, Nat. Commun. **6**, 8550 (2015).

[5] H. Thirumalai and J. R. Kitchin, Top. Catal. **61**, 462 (2018).

[6] G. X. Pei, X. Y. Liu, X. Yang, L. Zhang, A. Wang, L. Li, H. Wang, X. Wang, and T. Zhang, ACS Catal. **7**, 1491 (2017).

[7] C. M. Kruppe, J. D. Krooswyk, and M. Trenary, ACS Catal. **7**, 8042 (2017).

[8] P. Aich, H. Wei, B. Basan, A. J. Kropf, N. M. Schweitzer, C. L. Marshall, J. T. Miller, and R. Meyer, J. Phys. Chem. C **119**, 18140 (2015).

[9] M. Jørgensen and H. Grönbeck, J. Am. Chem. Soc. **141**, 8541 (2019).

[10] G. Giannakakis, M. Flytzani-Stephanopoulos, and E. C. H. Sykes, Acc. Chem. Res. **52**, 237 (2019).

[11] F. R. Lucci, M. T. Darby, M. F. G. Mattera, C. J. Ivimey, A. J. Therrien, A. Michaelides, M. Stamatakis, and E. C. H. Sykes, J. Phys. Chem. Lett. **7**, 480 (2016).

[12] Q. Fu and Y. Luo, ACS Catal. **3**, 1245 (2013).

[13] H. L. Tierney, A. E. Baber, J. R. Kitchin, and E. C. H. Sykes, Phys. Rev. Lett. **103**, 246102 (2009).

[14] A. E. Baber, H. L. Tierney, T. J. Lawton, and E. C. H. Sykes, ChemCatChem **3**, 607 (2011).

[15] G. Kyriakou, M. B. Boucher, A. D. Jewell, E. A. Lewis, T. J. Lawton, A. E. Baber, H. L. Tierney, M. Flytzani-Stephanopoulos, and E. C. H. Sykes, Science **335**, 1209 (2012).

[16] A. Borodziński and G. C. Bond, Catal. Rev. **48**, 91 (2006).

[17] M. M. Johnsson, D. W. Walker, and G. P. Nowack, U.S. patent 4,404,124 (12 September 1983).

[18] M. M. Johnsson and T. P. Cheung, U.S. patent 5,585,318 (16 December 1996).

[19] C. N. Thanh, B. Didillon, P. Sarrazin, and C. Cameron, U.S. patent 6,054,409 (24 April 2000).

[20] D. C. Huang, K. H. Chang, W. F. Pong, P. K. Tseng, K. J. Hung, and W. F. Huang, Catal. Lett. **53**, 155 (1998).

[21] N. A. Khan, S. Shaikhutdinov, and H.-J. Freund, Catal. Lett. **108**, 159 (2006).

[22] Q. Zhang, J. Li, X. Liu, and Q. Zhu, Appl. Catal., A **197**, 221 (2000).

[23] T. Bligaard and J. K. Nørskov, Electrochim. Acta **52**, 5512 (2007).

[24] R. J. Cole, N. J. Brooks, and P. Weightman, Phys. Rev. Lett. **78**, 3777 (1997).

[25] J. A. Rodriguez and D. W. Goodman, Science **257**, 897 (1992).

[26] I. A. Abrikosov, W. Olovsson, and B. Johansson, Phys. Rev. Lett. **87**, 176403 (2001).

[27] P. S. Bagus, E. S. Ilton, and C. J. Nelin, Surf. Sci. Rep. **68**, 273 (2013).

[28] M. Weinert and R. E. Watson, Phys. Rev. B **51**, 17168 (1995).

[29] S. Tougaard, J. Electron Spectrosc. Relat. Phenom. **178-179**, 128 (2010).

[30] M. T. Greiner, T. E. Jones, S. Beeg, L. Zwiener, M. Scherzer, F. Girgsdies, S. Piccinin, M. Armbrüster, A. Knop-Gericke, and R. Schlögl, Nat. Chem. **10**, 1008 (2018).

[31] S. Hüfner, G. K. Wertheim, and J. H. Wernick, Solid State Commun. **17**, 1585 (1975).

[32] D. van der Marel, J. A. Jullianus, and G. A. Sawatzky, Phys. Rev. B **32**, 6331 (1985).

[33] C. Norris and H. P. Myers, J. Phys. F: Met. Phys. **1**, 62 (1971).

[34] M. W. Haverkort, M. Zwierzycki, and O. K. Andersen, Phys. Rev. B **85**, 165113 (2012).

[35] P. Giannozzi, S. Baroni, N. Bonini, M. Calandra, R. Car, C. Cavazzoni, D. Ceresoli, G. L. Chiarotti, M. Cococcioni, I. Dabo, A. Dal Corso, S. De Gironcoli, S. Fabris, G. Fratesi, R. Gebauer, U. Gerstmann, C. Gougoussis, A. Kokalj, M. Lazzeri, L. Martin-samos, N. Marzari, F. Mauri, R. Mazzarello, S. Paolini, A. Pasquarello, L. Paulatto, and C. Sbraccia, J. Phys.: Condens. Matter **21**, 395502 (2009).

[36] A. Dal Corso, Comput. Mater. Sci. **95**, 337 (2014).

[37] I. Karakaya and W. T. Thompson, Bull. Alloy Phase Diagrams **9**, 237 (1988).

[38] E. G. Allison and G. C. Bond, Catal. Rev. **7**, 233 (1972).

[39] M. T. Darby, M. Stamatakis, A. Michaelides, and E. C. H. Sykes, J. Phys. Chem. Lett. **9**, 5636 (2018).

[40] M. T. Darby, E. C. H. Sykes, A. Michaelides, and M. Stamatakis, Top. Catal. **61**, 428 (2018).

[41] K. G. Papanikolaou, M. T. Darby, and M. Stamatakis, J. Phys. Chem. C **123**, 9128 (2019).

[42] P. T. Wouda, M. Schmid, B. E. Nieuwenhuys, and P. Varga, Surf. Sci. **417**, 292 (1998).

[43] J. S. Lim, J. Vandermause, M. A. van Spronsen, A. Musaelian, Y. Xie, L. Sun, C. R. O'Connor, T. Egle, N. Molinari, J. Florian, K. Duanmu, R. J. Madix, P. Sautet, C. M. Friend, and B. Kozinsky, J. Am. Chem. Soc. **142**, 15907 (2020).

[44] S. Doniach and M. Sunjic, J. Phys. C: Solid State Phys. **3**, 285 (1970).

[45] A. Bayer, K. Flechtner, R. Denecke, and H. Steinru, Surf. Sci. **600**, 78 (2006).

[46] G. M. McGuirk, J. Ledieu, É. Gaudry, M.-C. de Weerd, and V. Fournée, J. Chem. Phys. **141**, 084702 (2014).

[47] M. A. Van Spronsen, K. Daunmu, C. R. O'Connor, T. Egle, H. Kersell, J. Oliver-Meseguer, M. B. Salmeron, R. J. Madix, P. Sautet, and C. M. Friend, J. Phys. Chem. C **123**, 8312 (2019).

[48] H. Grönbeck, S. Klacar, N. M. Martin, A. Hellman, E. Lundgren, and J. N. Andersen, Phys. Rev. B **85**, 115445 (2012).

[49] P. Steiner and S. Hüfner, Acta Metall. **29**, 1885 (1981).

[50] M. Sigalas, D. A. Papaconstantopoulos, and N. C. Bacalis, Phys. Rev. B **45**, 5777 (1992).

[51] N. Taccardi, M. Grabau, J. Debuschewitz, M. Distaso, M. Brandl, R. Hock, F. Maier, C. Papp, J. Erhard, C. Neiss, W. Peukert, A. Görling, H.-P. Steinrück, and P. Wasserscheid, Nat. Chem. **9**, 862 (2017).

[52] G. Rupprechter, Nat. Chem. **9**, 833 (2017).

[53] L. Zhang, M. Zhou, A. Wang, and T. Zhang, Chem. Rev. **120**, 683 (2020).

[54] Y. Wang, B. Wang, L. Ling, R. Zhang, and M. Fan, Chem. Eng. Sci. **218**, 115549 (2020).

[55] S. González, K. M. Neyman, S. Shaikhutdinov, H.-J. Freund, and F. Illas, J. Phys. Chem. C **111**, 6852 (2007).

[56] D. Teschner, J. Borsodi, A. Wootsch, Z. Révay, M. Hävecker, A. Knop-Gericke, S. D. Jackson, and R. Schlögl, Science **320**, 86 (2008).

[57] F. Studt, F. Abild-Pedersen, T. Bligaard, R. Z. Sorensen, C. H. Christensen, and J. K. Norskov, Science **320**, 1320 (2008).

[58] D. Mei, M. Neurock, and C. M. Smith, J. Catal. **268**, 181 (2009).

[59] R. Qin, K. Liu, Q. Wu, and N. Zheng, Chem. Rev. **120**, 11810 (2020).

[60] I. Coulthard and T. K. Sham, Phys. Rev. Lett. **77**, 4824 (1996).

[61] G. Meitzner and J. H. Sinfelt, Catal. Lett. **30**, 1 (1994).

[62] E. Vignola, S. N. Steinmann, A. Al Farra, B. D. Vandegehuchte, D. Curulla, and P. Sautet, ACS Catal. **8**, 1662 (2018).

[63] E. Vignola, S. N. Steinmann, B. D. Vandegehuchte, D. Curulla, and P. Sautet, J. Phys. Chem. C **120**, 26320 (2016).

[64] E. Vignola, S. N. Steinmann, K. Le Mapihan, B. D. Vandegehuchte, D. Curulla, and P. Sautet, J. Phys. Chem. C **122**, 15456 (2018).

[65] V. Zhukov, K. Rendulic, and A. Winkler, Vacuum **47**, 5 (1996).

[66] M. T. Darby, R. Réocreux, E. C. H. Sykes, A. Michaelides, and M. Stamatakis, ACS Catal. **8**, 5038 (2018).

[67] M. Armbrüster, K. Kovnir, M. Behrens, D. Teschner, Y. Grin, and R. Schlögl, J. Am. Chem. Soc. **132**, 14745 (2010).

[68] Y. Luo, S. Alarcón Villaseca, M. Friedrich, D. Teschner, A. Knop-Gericke, and M. Armbrüster, J. Catal. **338**, 265 (2016).

[69] M. Armbrüster, M. Behrens, F. Cinquini, K. Föttinger, Y. Grin, A. Haghofer, B. Klötzer, A. Knop-Gericke, H. Lorenz, A. Ota, S. Penner, J. Prinz, C. Rameshan, Z. Révay, D. Rosenthal, G. Rupprechter, P. Sautet, R. Schlögl, L. Shao,

L. Szentmiklósi, D. Teschner, D. Torres, R. Wagner, R. Widmer, and G. Wowsnick, ChemCatChem **4**, 1048 (2012).

[70] M. Bron, D. Teschner, A. Knop-Gericke, F. C. Jentoft, J. Kröhnert, J. Hohmeyer, C. Volckmar, B. Steinhauer, R. Schlögl, and P. Claus, Phys. Chem. Chem. Phys. **9**, 3559 (2007).

[71] J. Hohmeyer, E. V. Kondratenko, M. Bron, J. Kröhnert, F. C. Jentoft, R. Schlögl, and P. Claus, J. Catal. **269**, 5 (2010).

[72] B. Delmon and G. F. Froment, Catal. Rev. - Sci. Eng. **38**, 69 (1996).

[73] R. Prins, Chem. Rev. **112**, 2714 (2012).

[74] G. D. Frey, V. Lavallo, B. Donnadieu, W. W. Schoeller, and G. Bertrand, Science **316**, 439 (2007).

[75] E. Baumgarten and E. Denecke, J. Catal. **95**, 296 (1985).

[76] J. Jia, K. Haraki, J. N. Kondo, K. Domen, and K. Tamaru, J. Phys. Chem. B **104**, 11153 (2000).